

Epsilon Canis Majoris: The Brightest EUV Source with Surprisingly Low Interstellar Absorption

J. Michael Shull^{1,2}, Rachel M. Curran², and Michael W. Topping³

(1) *Department of Astrophysical & Planetary Sciences,
University of Colorado; Boulder CO 80309, USA;*

(2) *Department of Physics and Astronomy,
University of North Carolina, Chapel Hill NC 27599, USA;*

(3) *Department of Astronomy, Steward Observatory,
University of Arizona, Tucson AZ 85721, USA*

michael.shull@colorado.edu, rcurran@unc.edu,
michaeltopping@arizona.edu

ABSTRACT

The B2 star ϵ CMa, at parallax distance $d = 124 \pm 2$ pc, dominates the H I photoionization of the local interstellar cloud (LIC). At its closer parallax distance compared to previous estimates, ϵ CMa has a 0.9 mag fainter absolute magnitude $M_V = -3.97 \pm 0.04$. We combine measurements of distance with the integrated flux $f = (41.5 \pm 3.3) \times 10^{-6}$ erg cm⁻² s⁻¹ and angular diameter $\theta_d = 0.80 \pm 0.05$ mas to produce a consistent set of stellar parameters: radius $R = 10.7 \pm 0.7 R_\odot$, mass $M = 13.1 \pm 2.3 M_\odot$, gravity $\log g = 3.50 \pm 0.05$, effective temperature $T_{\text{eff}} \approx 21,000$ K, and luminosity $L \approx 20,000 L_\odot$. These parameters place ϵ CMa outside the β Cephei instability strip, consistent with its observed lack of pulsations. The observed EUV spectrum yields a hydrogen photoionization rate $\Gamma_{\text{HI}} \approx 10^{-15}$ s⁻¹ (at Earth). The total flux decrement factor at the Lyman limit ($\Delta_{\text{LL}} = 5000 \pm 500$) is a combination of attenuation in the stellar atmosphere ($\Delta_{\text{star}} = 110 \pm 10$) and interstellar medium ($\Delta_{\text{ISM}} = 45 \pm 5$) with optical depth $\tau_{\text{LL}} = 3.8 \pm 0.1$. After correcting for interstellar H I column density $N_{\text{HI}} = (6 \pm 1) \times 10^{17}$ cm⁻², we find a stellar LyC photon flux $\Phi_{\text{LyC}} \approx 3000$ cm⁻² s⁻¹ and ionizing luminosity $Q_{\text{LyC}} = 10^{45.7 \pm 0.3}$ photons s⁻¹. The photoionization rate $\Gamma_{\text{H}} \approx (1-2) \times 10^{-14}$ s⁻¹ at the cloud surface produces an ionization fraction (30–40%) for total hydrogen density $n_{\text{H}} = 0.2$ cm⁻³. With its 27.3 ± 0.4 km s⁻¹ heliocentric radial velocity and small proper motion, ϵ CMa passed within 9.3 ± 0.5 pc of the Sun 4.4 Myr ago, with a 180 times higher photoionization rate.

1. Introduction to Properties of ϵ CMa

The B-type giant star Epsilon Canis Majoris (ϵ CMa), also known as HD 52089 and Adhara, is the brightest source of extreme ultraviolet (EUV) radiation in the sky (J. Dupuis et al. 1995; J. Vallergera & B. Welsh 1995) as observed by the Extreme Ultraviolet Explorer (EUVE). Because of the low-density interstellar medium (ISM) or “local interstellar tunnel” along its sight line (Gry et al. 1985; B. Welsh 1991; J. Cassinelli et al. 1995; J. Vallergera 1998; J. Linsky et al. 2019), this star dominates the local H I photoionization (J. Vallergera 1998), with a rate of $\Gamma_{\text{HI}} \approx 1.0 \times 10^{-15} \text{ s}^{-1}$ as viewed from Earth. Its spectrum, shown in Figure 1, has been measured by EUVE at $\lambda \leq 730 \text{ \AA}$, and more recently with the Colorado-DEUCE rocket at 700–1150 \AA (N. Erickson et al. 2021). The ionizing continuum flux outside the local interstellar clouds is considerably higher, after correcting for photoelectric absorption by H I ($\lambda \leq 912 \text{ \AA}$) and He I ($\lambda \leq 504 \text{ \AA}$).

In a classic survey of southern B-type stars, J. Lesh (1972) listed the spectral type (SpT) of ϵ CMa as B2 II, with apparent and absolute visual magnitudes ($m_V = 1.50$, $M_V = -4.9$) and a spectrophotometric distance of 187 pc. In later papers, the distance to ϵ CMa was quoted variously as 179 pc (R. Bohlin 1975) and 188 pc (e.g., T. Snow & D. Morton 1976; B. Savage et al. 1977; R. Bohlin et al. 1978; J. Cassinelli et al. 1995). However, the *Hipparcos* parallax measurement of $8.05 \pm 0.14 \text{ mas}$ (F. van Leeuwen 2007) provided a shorter distance $d = 124 \pm 2 \text{ pc}$, with distance modulus ($m_V - M_V$) = 5.467 ± 0.035 smaller by 0.90 mag than for 188 pc. The observed visual magnitude $m_V = 1.50$ implies an absolute magnitude $M_V = -3.97 \pm 0.04$, also 0.9 mag fainter than the value of -4.9 given in J. Lesh (1972) for B2 II type. The luminosity gap is even larger for the recent classification as B1.5 II (L. Fossati et al. 2015) with $M_V = -5.1$. Unless the parallax measurements are wrong, the star is underluminous for its morphologically classified spectral type.

In this paper, we investigate the stellar parameters of ϵ CMa and the attenuation of its ionizing spectrum. Using non-LTE, line-blanketed model atmospheres for the stellar EUV continuum and flux decrement at the Lyman limit (LL), we determine the attenuation of the EUV in both the stellar atmosphere and ISM. In Section 2, we derive a new set of stellar parameters (radius, mass, effective temperature, luminosity) consistent with measurements of the parallax distance, stellar angular diameter, and total flux. In Section 3, we analyze the absorption in the stellar atmosphere and intervening ISM. We find an interstellar H I column density $N_{\text{HI}} = (6 \pm 1) \times 10^{17} \text{ cm}^{-2}$, corresponding to a LL optical depth $\tau_{\text{LL}} = 3.8 \pm 0.1$ and a flux decrement of a factor of $\Delta_{\text{ISM}} = 45 \pm 5$. Combined with a decrement $\Delta_{\text{star}} = 110 \pm 10$ in the stellar atmosphere, the total decrement $\Delta_{\text{LL}} = 5000$ is consistent with the EUV observations. In Section 4, we discuss the implications of our results for the ionization structure of the local interstellar clouds.

2. Revised Stellar Parameters

2.1. Implications of the Closer Distance

A key measurement for ϵ CMa is its angular diameter $\theta_d = 0.80 \pm 0.05$ mas (R. Hanbury Brown et al. 1974) using the stellar interferometer at the Narrabri Observatory. From this and the parallax distance $d = 124 \pm 2$ pc, we derive a stellar radius of

$$R = \left(\frac{\theta_d d}{2} \right) = 7.42 \times 10^{11} \text{ cm} \quad (10.7 \pm 0.7 R_\odot), \quad (1)$$

where we combined the relative errors on θ_d (6.3%) and d (1.7%) in quadrature. This “interferometric radius” is considerably smaller than previous values in the literature, and the revision in stellar distance from 188 pc to 124 pc will alter many stellar properties.

The first change is the reduction in stellar radius to $10.7 R_\odot$, previously listed as $16.6 R_\odot$ (T. Snow & D. Morton 1976) and $16.2 \pm 1.2 R_\odot$ (J. Cassinelli et al. 1995). L. Fossati et al. (2015) adopted $d = 124 \pm 2$ pc and evaluated the radius and mass from two sets of evolutionary models: $R = 12.0_{-1.5}^{+1.7} R_\odot$ and $M = 13.1_{-0.9}^{+1.0} M_\odot$ (tracks from C. Georgy et al. 2013) and $R = 10.1_{-0.5}^{+0.7} R_\odot$ and $M = 12.0_{-0.4}^{+0.4} M_\odot$ (tracks from L. Brott et al. 2011). The new parallax distance implies a fainter absolute magnitude and suggests that its luminosity class might be II/III (giant) rather than II (bright giant) derived from its spectral morphology (L. Fossati et al. 2015; I. Negueruelo et al. 2024). This would be consistent with its smaller interferometric radius.

A second change concerns the elevated EUV fluxes from ϵ CMa. J. Cassinelli et al. (1995) noted that these fluxes are an order of magnitude larger than predicted by model stellar atmospheres, both LTE (R. Kurucz 1979) and non-LTE (I. Hubeny et al. 1994). Using high-resolution spectra, L. Fossati et al. (2015) changed the stellar classification from B2 II to B1.5 II, raised the effective temperature from $T_{\text{eff}} = 20,990 \pm 760$ K (A. Code et al. 1976) to $22,500 \pm 300$ K, and increased the surface gravity from $\log g = 3.20$ to 3.40 ± 0.08 . A recent study of spectral classifications of B-type stars (I. Negueruela et al. 2024) also listed ϵ CMa as B1.5 II, based on morphological comparison of its optical spectrum with other B-star standards. However, as discussed below (Section 2.3), the higher T_{eff} is inconsistent with the bolometric relation between stellar integrated flux and surface area, $T_{\text{eff}} = (L/4\pi R^2 \sigma_{\text{SB}})^{1/4}$. A value $T_{\text{eff}} = 21,000$ K is more consistent with the bolometric luminosity and radius. However, because of the back-warming effects of a stellar wind, a model-atmosphere temperature of $22,500$ K may be needed to interpret the elevated EUV continuum fluxes. In Section 2.3 we examine the stellar parameters (M , R , g , T_{eff}) required for consistency with the integrated flux f , luminosity L , and bolometric magnitude M_{bol} .

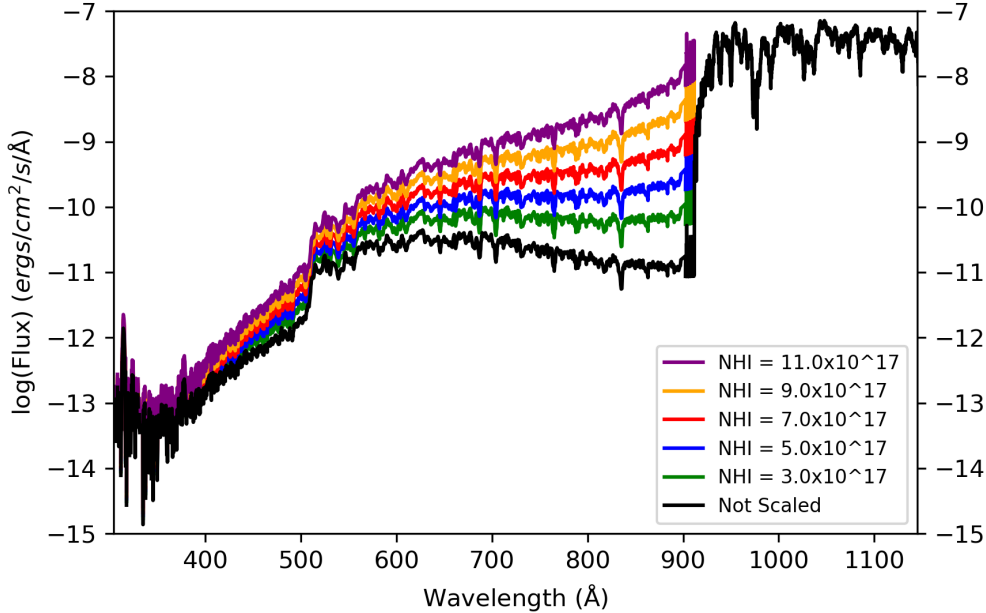


Fig. 1.— The lowest curve (black) shows the flux-calibrated spectrum of ϵ CMa (N. Erickson et al. 2021), a combination of data from the DEUCE rocket flight and previous EUVE and IUE data to which DEUCE was scaled. The five higher curves show restored continua for column densities $N_{\text{HI}} = (3\text{--}11)\times 10^{17} \text{ cm}^{-2}$ and $N_{\text{HeI}} = 0.06 N_{\text{HI}}$ based on observed elevated He^+ ionization fractions. These curves multiply the observed fluxes by $\exp(\tau_\lambda)$ for optical depths τ_λ in the ionizing continua of H I ($\lambda \leq 912 \text{ \AA}$) and He I ($\lambda \leq 504 \text{ \AA}$). The factor of 5000 ± 500 flux decrement at 912 \AA (black curve) is a combination of a (110 ± 10) decrement in the stellar atmosphere and a (45 ± 5) decrement from interstellar absorption. We then infer an ISM optical depth $\tau_{\text{LL}} = 3.8 \pm 0.1$ at the 912 \AA edge and $N_{\text{HI}} = (6 \pm 1) \times 10^{17} \text{ cm}^{-2}$.

2.2. Absolute Magnitude and Classification of ϵ CMa.

The absolute magnitude and bolometric magnitude of ϵ CMa need revision, consistent with its closer distance $d = 124 \pm 2 \text{ pc}$. The observed visual magnitude $m_V = 1.50$ corresponds to absolute magnitude $M_V = -3.97 \pm 0.04$. The stellar classification of B1.5 II (L. Fossati et al. 2015) and $M_V = -5.1$ from J. Lesh (1968) interpolated to B1.5 II results in a large distance discrepancy, with $(m_V - M_V) = 6.6$ and $d = 209 \text{ pc}$. In a compilation of absolute magnitudes for OB stars (Table 11 in D. Bowen et al. 2008) the recommended values of $M_V = -4.7$ (B2 II) and $M_V = -4.9$ (B1.5 II) differ slightly from those in J. Lesh (1968). However, these also imply unacceptably large distances: $(m_V - M_V) = 6.20$ ($d = 173 \text{ pc}$) for B2 II and $(m_V - M_V) = 6.40$ ($d = 190 \text{ pc}$) for B1.5 II.

Absolute magnitudes change rapidly with luminosity class at spectral types B1–B2. Classifications of B2 II ($M_V = -4.9$) and B2 III ($M_V = -3.3$) straddle the observational value of ϵ CMa ($M_V \approx -4.0$). We therefore suggest that ϵ CMa may be luminosity class B2 II/III rather than B2 II, providing a consistent bolometric magnitude with distance modulus ($m_V - M_V$) = 5.467 ($d = 124$ pc) and $M_V = -3.97$. For reference, the solar absolute bolometric magnitude $M_{\text{bol},\odot} = 4.74$ corresponds to luminosity $L_\odot = 3.828 \times 10^{33}$ erg s $^{-1}$. Figure 5 in M. Pedersen et al. (2020) shows a bolometric correction ($M_{\text{bol}} - M_V$) = -2.0 for $\log g = 3.5$ and $T_{\text{eff}} = 21,000$ K, leading to a bolometric absolute magnitude $M_{\text{bol}} = -5.97$ and $L = 19,200 L_\odot$. In contrast, the bolometric correction at $T_{\text{eff}} = 22,500$ K is -2.2 , yielding $M_{\text{bol}} = -6.17$ and $L = 23,000 L_\odot$. The 16% larger luminosity arises from a mismatch between the bolometric temperature and the elevated temperature (22,500 K) invoked to produce the EUV continuum.

2.3. Stellar Luminosity and Effective Temperature

The discrepancy between spectrophotometric and parallax distances requires revising M_V and M_{bol} for ϵ CMa. Consistent values of R , T_{eff} , M_{bol} , and L must satisfy the relations $g = (GM/R^2)$ and $L = 4\pi R^2 \sigma_{\text{SB}} T_{\text{eff}}^4$, where $\sigma_{\text{SB}} = 5.6704 \times 10^{-5}$ erg cm $^{-2}$ s $^{-1}$ K $^{-4}$ is the Stefan-Boltzmann constant and $R = (\theta_d d/2)$. Here, $\theta_d = 3.88 \times 10^{-9}$ rad (0.80 ± 0.05 mas) is the measured stellar angular diameter (R. Hanbury Brown et al. 1974). The integrated stellar flux is $f = (41.5 \pm 3.3) \times 10^{-6}$ erg cm $^{-2}$ s $^{-1}$ from A. Code et al. (1976), who combined ground-based visual and near-infrared photometry with ultraviolet observations (1100–3500 Å) taken by the Orbiting Astronomical Observatory (OAO-2). This flux included an extrapolated value for shorter wavelengths $f(\lambda \leq 1100 \text{ Å}) = 6.5 \times 10^{-6}$ erg cm $^{-2}$ s $^{-1}$, in agreement with the flux-calibrated DEUCE rocket observations from 700–1150 Å (N. Erickson et al. 2021). Even after correcting the observed EUV flux for interstellar absorption, the Lyman continuum represents less than 1% of the bolometric flux.

The constraints from stellar angular diameter and total flux give a useful relation for the bolometric effective temperature $T_{\text{eff}} = (4f/\sigma_{\text{SB}} \theta_d^2)^{1/4}$ or

$$T_{\text{eff}} = (21,000 \pm 780 \text{ K}) \left(\frac{f}{41.5 \times 10^{-6}} \right)^{1/4} \left(\frac{\theta_d}{0.80 \text{ mas}} \right)^{-1/2}. \quad (2)$$

From the stellar radius and bolometric T_{eff} , we find the total luminosity,

$$L = (19,900 L_\odot) \left(\frac{T_{\text{eff}}}{21,000 \text{ K}} \right)^4 \left(\frac{R}{10.7 R_\odot} \right)^2, \quad (3)$$

which agrees by construction with the relation $L = 4\pi d^2 f$. With the relative errors on parallax distance (1.7%) and integrated flux (8%), the luminosity is known to 8.2%. Given

the accuracy of the integrated flux and distance, we will maintain the bolometric value $T_{\text{eff}} = 21,000$ K. However, as discussed in Section 2.4, the elevated model temperature of 22,500 K from stellar-wind backwarming may provide a better fit to the EUV continuum and stellar flux decrement at the Lyman limit. Table 1 summarizes the stellar parameters used in previous papers, together with our revised values.

2.4. Stellar Atmospheres and EUV Fluxes

Two problems remain in understanding the elevated EUV fluxes from ϵ CMa and in reconciling the two values of T_{eff} (21,000 K and 22,500 K) frequently quoted in the literature. J. Cassinelli et al. (1995) noted that “the emergent flux from ϵ CMa in the hydrogen Lyman continuum exceeds the value expected from model atmospheres by a factor of about 30, even when the effects of line blanketing are accounted for.” Because this discrepancy was found in both LTE and non-LTE model atmospheres with $T_{\text{eff}} = 21,000$ K, they suggested that backwarming by the shocked stellar wind could boost the temperature in the upper atmosphere where the Lyman continuum is formed. A similar non-LTE wind effect was proposed by F. Najarro et al. (1996), involving doppler shifts and velocity-induced changes in density that affect the escape of H I and He I resonance lines and their ground-state populations. Both mechanisms are sensitive to mass-loss rates in the range $\dot{M} \approx (1-10) \times 10^{-9} M_{\odot} \text{ yr}^{-1}$.

J. Cassinelli et al. (1995) compared the observed fluxes of ϵ CMa to model atmospheres with $T_{\text{eff}} = 21,000$ K and $\log g = 3.20$ ($g = 1585 \text{ cm s}^{-2}$) and adopted $M = 15.2 M_{\odot}$ and $R = 16.2 R_{\odot}$. In their spectroscopic analysis of ϵ CMa, L. Fosatti et al. (2015) derived $\log g = 3.40 \pm 0.08$ and spectral type B1.5 II. In this paper, for consistency with the parameter changes (radius, distance, interferometric diameter), we increased $\log g$ to 3.50 ± 0.05 ($g = GM/R^2 = 3162 \text{ cm s}^{-2}$). The rotational velocity has been measured at $V_{\text{rot}} \sin i = 21.2 \pm 2.2 \text{ km s}^{-1}$ (Fosatti et al. 2015). With $R = 10.7 \pm 0.7 R_{\odot}$, we can safely neglect the centrifugal term, $V_{\text{rot}}^2/R \approx (6 \text{ cm s}^{-2})(\sin i)^{-2}$ and infer a gravitational mass ($M = gR^2/G$) of

$$M = (13.1 \pm 2.3 M_{\odot}) \left(\frac{g}{3162 \text{ cm s}^{-2}} \right) \left(\frac{R}{10.7 R_{\odot}} \right)^2. \quad (4)$$

The quoted error on M includes uncertainties in surface gravity and radius, added in quadrature with $(\sigma_M/M)^2 = (\sigma_g/g)^2 + (2\sigma_R/R)^2$.

The position of ϵ CMa on the Hertzsprung-Russell (H-R) diagram is shown in Figure 2, with our revised parameters, $\log(L/L_{\odot}) = 4.30$ and $T_{\text{eff}} = 21,000$ K, and evolutionary tracks from Brott et al. (2011). Its position falls close to the $12 M_{\odot}$ track, not far from our mass estimate in eq. (4) with $R = 10.7 R_{\odot}$ and $\log g = 3.5$. A lower value ($\log g = 3.40 \pm 0.08$)

would reduce the gravitational mass to $10.4 \pm 2.5 M_{\odot}$. This H-R position is consistent with luminosity class II/III (giant) rather than class II (bright giant). It also places ϵ CMa out of the β Cephei instability strip, consistent with the lack of observed pulsations. This conclusion was confirmed by comparison with the locus of radial and non-radial instability modes shown in Figures 2 and 3 of L. Deng & D. R. Xiong (2001).

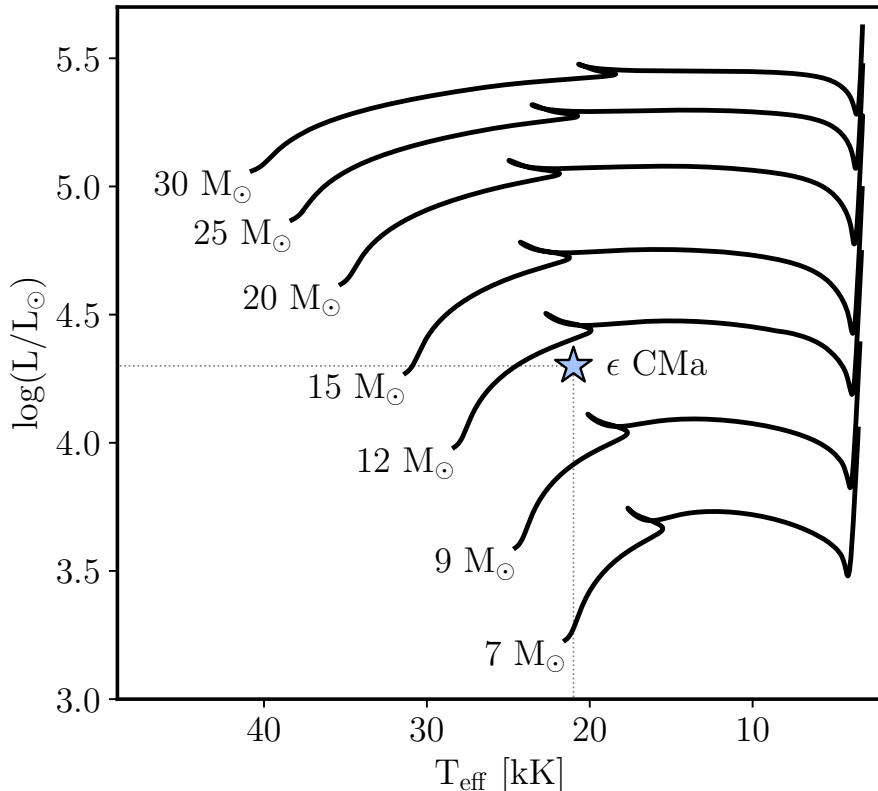


Fig. 2.— The location of ϵ CMa on the Hertzsprung-Russell diagram is shown for our revised parameters, $\log(L/L_{\odot}) = 4.30$ and $T_{\text{eff}} = 21,000$ K, based on new radius $R = 10.7 R_{\odot}$ (for $d = 124$ pc). The evolutionary tracks are from Brott et al. (2011) with Milky Way metallicities and initial masses labeled from 7–30 M_{\odot} .

3. Interstellar Absorption and H I Column Density

3.1. Previous Column Density Estimates

Figure 1 shows the flux-calibrated FUV and EUV spectra of ϵ CMa taken by EUVE (J. Dupuis et al. 1995) and the Colorado-DEUCE rocket (N. Erickson et al. 2021). The

continuum flux drops by a factor $\Delta_{\text{LL}} = 5000 \pm 500$ at the 912 Å Lyman limit, with a further decrease at the He I photoionization edge (504 Å). The total optical depth at 912 Å is $\tau_{\text{LL}} = \ln \Delta_{\text{LL}}$. Some attenuation is intrinsic to the stellar atmosphere, owing to H I opacity that varies with SpT and T_{eff} . Additional photoelectric absorption occurs in the ISM. The fact that ϵ CMa is a strong source of local EUV radiation is largely a result of its location in a low-density cavity or local interstellar tunnel.

Past estimates for the amount of interstellar hydrogen toward ϵ CMa span a wide range (Table 2). Using *Copernicus* ultraviolet spectral fits to the wings of the interstellar Ly α absorption line, R. Bohlin (1975) set an upper limit of $N_{\text{HI}} < 5 \times 10^{18} \text{ cm}^{-2}$, corresponding to optical depth $\tau_{\text{LL}} < 31.5$. The actual ISM column density is much less, since detectable EUV flux makes it through the local clouds to Earth. Because Ly α absorption measurements are uncertain at low H I column densities, several groups have estimated N_{HI} by scaling from column densities of heavy elements believed to co-exist with H I. Using ultraviolet spectra taken with the G160M grating (resolving power $R \approx 20,000$) of the Goddard High Resolution Spectrograph (GHRS) aboard the Hubble Space Telescope (HST), C. Gry et al. (1995) estimated that $N_{\text{HI}} < 5 \times 10^{17} \text{ cm}^{-2}$ scaled from N I absorption lines. This estimate required assumptions about the gas-phase metallicities and possible corrections for depletion onto dust grains. They used a mean interstellar nitrogen abundance of $10^{-4.17}$ relative to hydrogen found by R. Ferlet (1981) in unreddened sight lines observed by *Copernicus*. They also noted difficulties produced by blending of the interstellar N I (1199–1200 Å) triplet absorption lines with narrow stellar features.

An improved analysis by C. Gry & E. Jenkins (2001) used HST observations of ultraviolet absorption lines of N I, O I, and S II taken with the echelle grating of GHRS ($R \sim 100,000$). The increased spectral resolution and high signal-to-noise ratio of these data allowed them to identify three principal velocity components at heliocentric velocities 17, 10, and -10 km s^{-1} , previously referred to as Components 1, 2, and 3. Component 1 is known as the Local Interstellar Cloud (LIC) and Component 2 is called the Blue Cloud, also seen in absorption toward Sirius ($d = 2.64 \text{ pc}$). Scaling from N I, they estimated a range of H I column densities $N_{\text{HI}} = (3.1\text{--}3.7) \times 10^{17} \text{ cm}^{-2}$. They quoted two estimates scaled from O I, with $N_{\text{HI}} = (7\text{--}11) \times 10^{17} \text{ cm}^{-2}$ for $\text{O}/\text{H} = 3.16 \times 10^{-4}$ and $N_{\text{HI}} = (4.8\text{--}7.2) \times 10^{17} \text{ cm}^{-2}$ for $\text{O}/\text{H} = 4.68 \times 10^{-4}$. The difference in these estimates (see Table 2) reflects their assumptions about (N/H and O/H) abundances and possible depletion into grains. The offset between N and O scalings could indicate sub-solar interstellar nitrogen abundances. A N I deficiency in the local ISM was noted by E. Jenkins et al. (2000) from far-UV spectra of white dwarf stars observed with FUSE. However, in a survey of B-type stars, M.-F. Nieva & N. Przybilla (2012) noted that ϵ CMa had a slightly elevated stellar N/H abundance (0.2–0.3 dex) compared to unmixed B stars in the solar neighborhood.

3.2. Photoelectric Absorption

In this section, we derive N_{HI} by comparing the observed EUV continuum fluxes to estimates of the stellar continuum (non-LTE model atmospheres) and attenuation by the ISM. We restore the observed continuum to its shape at the stellar surface by multiplying the observed flux by $\exp(\tau_\lambda)$, using optical depths $\tau(\lambda)$ of photoelectric absorption in the ionizing continua of H I ($\lambda \leq 912 \text{ \AA}$) and He I ($\lambda \leq 504 \text{ \AA}$),

$$\tau_{\text{HI}}(\lambda) \approx (0.630) \left(\frac{N_{\text{HI}}}{10^{17} \text{ cm}^{-2}} \right) \left(\frac{\lambda}{912 \text{ \AA}} \right)^3, \quad (5)$$

$$\tau_{\text{HeI}}(\lambda) \approx (0.737) \left(\frac{N_{\text{HeI}}}{10^{17} \text{ cm}^{-2}} \right) \left(\frac{\lambda}{504 \text{ \AA}} \right)^{1.63}. \quad (6)$$

These approximations are based on power-law fits to the photoionization cross sections at wavelengths below threshold, $\sigma_{\text{HI}}(\lambda) \approx (6.30 \times 10^{-18} \text{ cm}^2)(\lambda/912 \text{ \AA})^3$ (D. Osterbrock & G. Ferland 2006) and $\sigma_{\text{HeI}}(\lambda) \approx (7.37 \times 10^{-18} \text{ cm}^2)(\lambda/504 \text{ \AA})^{1.63}$ (D. Samson et al. 1994). In our actual calculations, we used the exact (non-relativistic) H I cross section (Bethe & Salpeter 1957), which has frequency dependence,

$$\sigma_\nu = \sigma_0 \left(\frac{\nu}{\nu_0} \right)^{-4} \frac{\exp[4 - (4 \arctan \epsilon)/\epsilon]}{[1 - \exp(-2\pi/\epsilon)]}. \quad (7)$$

Here, the dimensionless parameter $\epsilon \equiv [(\nu/\nu_0) - 1]^{1/2}$ with frequency ν_0 defined at the ionization energy $h\nu_0 = 13.598 \text{ eV}$ and $\sigma_0 = 6.304 \times 10^{-18} \text{ cm}^2$. The two formulae agree at threshold $\nu = \nu_0$, but the approximate formula deviates increasingly at shorter wavelengths. The exact cross section is higher by 8.2% (700 \AA), 12.3% (600 \AA), and 16.4% (500 \AA). In our models, we found that the exact cross section increased the photoionization rates by 10–13% in models with $N_{\text{HI}} = (3\text{--}8) \times 10^{17} \text{ cm}^{-2}$.

The flux-restoration method for inferring ISM opacities from the observed EUV flux has inherent uncertainties. It requires accurate model-atmosphere estimates of the flux decrement factor Δ_{star} at the Lyman limit and the shape of the EUV continuum below the ionization edge. Especially important are non-LTE treatments of the H I and He I abundances in their ($1s$ and $1s^2$) ground states and possible back-warming effects of stellar winds. J. Cassinelli et al. (1995) noted that EUVE fluxes in both H I and He I continua were significantly greater than predicted by both LTE and non-LTE model atmospheres. They quoted a wide range of $N_{\text{HI}} = (0.7\text{--}1.2) \times 10^{18} \text{ cm}^{-2}$.

To improve on this technique, we followed a similar procedure, calculating the interstellar opacities of both H I and He I. In the flux-calibrated data (Figure 1) the far-UV stellar continuum rises slowly from 1000 \AA down to 912 \AA , owing to absorption in higher Lyman-series lines converging on the LL at 911.75 \AA . We estimate the extrapolated continuum level

at 912^+ \AA , longward of the edge, as $F_\lambda = 5 \times 10^{-8} \text{ erg cm}^{-2} \text{ s}^{-1} \text{ \AA}^{-1}$, dropping by a factor $\Delta_{\text{LL}} \approx 5000 \pm 500$ to $1.0 \times 10^{-11} \text{ erg cm}^{-2} \text{ s}^{-1} \text{ \AA}^{-1}$ just below the Lyman edge.

We compared these restored continua to the EUV continuum shape and the Lyman flux decrement in model atmospheres, using the code `WM-basic` developed by A. Pauldrach et al. (2001)¹. We chose this code because of its hydrodynamic solution of expanding atmospheres with line blanketing and non-LTE radiative transfer, including its treatment of the continuum and wind-blanketing from EUV lines. This code was the standard for atmosphere modeling in the population synthesis code `Starburst99` (C. Leitherer et al. 1999, 2014) and used by M. Topping & J. M. Shull (2015) to evaluate the production rate of Lyman continuum radiation in OB-stars. Extensive discussion of hot-star atmosphere codes appears in papers by D. J. Hillier & D. Miller (1998), F. Martins et al. (2005), and C. Leitherer et al. (2014).

3.3. Combined Stellar and Interstellar Absorption

The restored EUV continua shown in Figure 1 covered the range of interstellar H I column densities, $(3\text{--}11) \times 10^{17} \text{ cm}^{-2}$, quoted in the literature. After correcting for photoelectric absorption of the EUVE and DEUCE fluxes, we found that values $N_{\text{HI}} \geq 9 \times 10^{17} \text{ cm}^{-2}$ are inconsistent with the observed flux decrements at the Lyman edge, based on model atmospheres and using the exact H I cross section in equation (7). We narrowed our study to interstellar H I column densities in the range $(5\text{--}8) \times 10^{17} \text{ cm}^{-2}$.

The total flux decrement factor Δ_{LL} at the Lyman limit is the combination of attenuation in the stellar atmosphere (Δ_{star}) and the interstellar medium (Δ_{ISM}). We constrain the product of stellar and interstellar attenuation factors by finding the optical depth ($\tau_{\text{ISM}} = \ln \Delta_{\text{ISM}}$) at the 912 \AA edge consistent with the range of LL decrements found in a set of model atmospheres run for B1.5–B2 giants ($T_{\text{eff}} = 21,000\text{--}22,500 \text{ K}$ and $\log g = 3.4\text{--}3.5$). Because LL optical depth depends logarithmically on the H I column density, values of τ_{LL} provide better constraints on N_{HI} than broad-band fits between $504\text{--}912 \text{ \AA}$. As described below, we adopted a combination of $\Delta_{\text{star}} = 110 \pm 10$ and $\Delta_{\text{ISM}} = 45 \pm 5$ to produce a total decrement of $\Delta_{\text{LL}} = \Delta_{\text{star}} \times \Delta_{\text{ISM}} = 5000 \pm 500$.

Figure 3 shows the FUV/EUV fluxes and Lyman flux decrements for three non-LTE, line-blanketed model atmospheres. Two models adopt $T_{\text{eff}} = 22,500 \text{ K}$, the elevated temperature proposed by L. Fossati et al. (2015), with $\log g = 3.40$ and 3.50 . A third model assumes $T_{\text{eff}} = 21,000 \text{ K}$ and $\log g = 3.50$, consistent with the bolometric relations between integrated

¹This code can be found at <http://www.usm.uni-muenchen.de/people/adi/Programs/Programs.html>

flux and angular diameter (see eq. 2). The hotter models with stellar winds include backwarming of the star’s outer atmosphere, which raises the temperatures where the emergent ionizing continua of H I and He I are produced. The two 22,500 K (**WM-basic**) models exhibit LL decrements Δ_{star} of 102 and 119. We also analyzed decrements in two CMFGEN model atmospheres (D. J. Hillier & D. Miller 1998) with $T_{\text{eff}} = 22,500$ K and $\log g = 3.50$, provided by D. J. Hillier (private communication). These models include stellar winds with mass-loss rates of $1\text{--}4 \times 10^{-9} M_{\odot} \text{ yr}^{-1}$ and produce LL decrements $\Delta_{\text{star}} \approx 120 - 140$.

We adopt a stellar decrement $\Delta_{\text{star}} = 110 \pm 10$ based on **WM-basic** models (see Figure 3). To produce the observed total Lyman decrement $\Delta_{\text{LL}} = 5000 \pm 500$, the ISM generate an additional decrement $\Delta_{\text{ISM}} = 45 \pm 5$, corresponding to optical depth $\tau_{\text{LL}} = 3.8 \pm 0.1$ and H I column density $N_{\text{HI}} = (6 \pm 1) \times 10^{17} \text{ cm}^{-2}$. We estimate 10% uncertainty in defining the continuum longward of 912 Å and 15% uncertainty in the LL decrement in the model atmospheres. Because of the weak scaling of optical depth with flux decrement ($\tau_{\text{LL}} = \ln \Delta_{\text{LL}}$) the uncertainties on τ_{ISM} and column density N_{HI} are small. Figure 4 shows the observed and restored EUV continua for our constrained H I column density, overlaid with the stellar atmosphere model with decrement $\Delta_{\text{LL}} = 102$. The combined stellar and interstellar decrements are in good agreement with the flux-restored EUV spectrum from 912 Å down to 750 Å. The model atmosphere falls below the restored continuum from 750 Å down to 504 Å, but it fits the He I continuum quite well at $\lambda < 504$ Å.

Table 3 summarizes the results of our models of the restored ionizing continua for a range of column densities. These parameters include the integrated photon flux Φ_{LyC} , photoionization rate Γ_{HI} , Lyman decrement Δ_{ISM} , and the hydrogen ionization fraction at the outer surface of the local cloud. In photoionization equilibrium, these fractions, $x = (1/2)[-a + (a^2 + 4a)^{1/2}]$, are the solution of $x^2/(1 - x) = a$, where $a = \Gamma_{\text{H}}/(1.1n_{\text{H}}\alpha_{\text{H}})$. We included a factor 1.1 for electrons contributed by He^+ , although helium may be somewhat more ionized than hydrogen owing to contributions from hot white dwarfs and EUV emission lines produced in the hot local bubble. The local cloud is assumed to have constant hydrogen density $n_{\text{H}} \equiv n_{\text{HI}} + n_{\text{HII}} \approx 0.2 \text{ cm}^{-3}$ with a hydrogen case-B radiative recombination coefficient $\alpha_{\text{H}} = 3.39 \times 10^{-13} \text{ cm}^3 \text{ s}^{-1}$ at $T = 7000$ K. For our best fit, $N_{\text{HI}} = (6 \pm 1) \times 10^{17} \text{ cm}^{-2}$, the EUV radiation field outside the local clouds is 10–20 times higher than viewed from Earth, with $\Phi_{\text{LyC}} \approx 3000 \pm 1000 \text{ photons cm}^{-2} \text{ s}^{-1}$ and $\Gamma_{\text{H}} = (1\text{--}2) \times 10^{-14} \text{ s}^{-1}$. At the outer surface of the local clouds exposed to the higher LyC flux, hydrogen is partially ionized, with ionization fractions $x_s \approx 30\text{--}40\%$ for $n_{\text{H}} = 0.2 \text{ cm}^{-3}$. Somewhat higher fractions are found if we reduce the density to $n_{\text{H}} = 0.1 \text{ cm}^{-3}$.

4. Summary of Results and Future Studies

We have derived a new set of stellar parameters for ϵ CMa (mass, radius, effective temperature, luminosity) consistent with its shorter parallax distance (124 pc vs. 188 pc), interferometric angular diameter ($\theta_d = 0.80 \pm 0.05$ mas), and integrated bolometric flux, $f = (41.5 \pm 3.3) \times 10^{-6}$ erg cm $^{-2}$ s $^{-1}$. From these, we derive $T_{\text{eff}} = 21,000 \pm 780$ K and $L \approx 20,000 L_{\odot}$. With updated absolute magnitudes ($M_V = -3.97 \pm 0.04$ and $M_{\text{bol}} = -5.97$) ϵ CMa is sub-luminous by 0.9–1.1 mag for its morphological classification as a bright giant, either B2 II (Lesh 1972) or B1.5 II (Fossati et al. 2015), and it has inconsistent values of R , T_{eff} , d , and radiative flux. On the H-R diagram, the new parameters shift ϵ CMa out of the β -Cephei pulsational instability strip, consistent with its observed lack of pulsations and the boundaries of theoretical instability on evolutionary tracks (L. Deng & D. R. Xiong 2001).

The following points summarize our primary results:

1. The combination of parallax distance and angular diameter yield a stellar radius $R = 10.7 \pm 0.7 R_{\odot}$ and luminosity $L \approx 20,000 L_{\odot}$, both smaller than previous estimates. Bolometric relations between flux and radius suggest an effective temperature $T_{\text{eff}} \approx 21,000 \pm 780$ K and absolute magnitude $M_V = -3.97 \pm 0.04$, appropriate for a B2 II/III star. A previous spectroscopic analysis (Fossati et al. 2015) gives $T_{\text{eff}} = 22,500$ K at SpT = B1.5 II.
2. From models of the stellar and interstellar attenuation of the ionizing flux in the Lyman continuum ($\lambda \leq 912 \text{ \AA}$) we determine a column density $N_{\text{HI}} = (6 \pm 1) \times 10^{17} \text{ cm}^{-2}$. This measurement agrees with values (C. Gry et al. 2001) scaled from HST-observed column densities of O I, but not with N I. The differences could arise from ionization effects or assumed metallicities in the local ISM.
3. Using non-LTE model atmospheres and observed EUV spectra, we estimate LL flux decrements $\Delta_{\text{star}} = 110 \pm 10$ and $\Delta_{\text{ISM}} = 45 \pm 5$, in agreement with the observed total decrement $\Delta_{\text{LL}} = 5000 \pm 500$. The restored ionizing continuum of ϵ CMa outside the local clouds has photon flux $\Phi_{\text{LyC}} \approx 3000 \pm 1000 \text{ cm}^{-2} \text{ s}^{-1}$ and ionizing photon luminosity $Q_{\text{LyC}} \approx 10^{45.7 \pm 0.3} \text{ photons s}^{-1}$ for $d = 124 \pm 2$ pc.
4. The H I column density for the local cloud corresponds to optical depth $\tau_{\text{LL}} = 3.8 \pm 0.1$ at the Lyman limit. The EUV flux external to the local clouds is 10–20 times higher than viewed from Earth, with a photoionization rate $\Gamma_{\text{H}} \approx (1\text{--}2) \times 10^{-14} \text{ s}^{-1}$. At the cloud surface, hydrogen would be partially ionized, with ionization fraction $x \approx 30\text{--}40\%$ in gas with $n_{\text{H}} = 0.2 \text{ cm}^{-3}$ and $T \approx 7000$ K.

Future work. With an accurate interstellar H I column density to ϵ CMa, the next step will be the development of 3D photoionization models of H, He, and heavy elements in the local clouds. As shown previously (J. Dupuis et al. 1995; J. Vallergera & B. Welsh 1995) the EUV radiation field, as viewed from Earth, is dominated by five stellar sources: two early B-type stars (ϵ CMa and β CMa) and three bright white dwarf stars (G191-B2B, HZ 43, Feige 24). While ϵ CMa is the dominant EUV source in the H I ionizing band (504–912 Å), the white dwarfs and EUV emission lines from surrounding hot gas dominate the EUV spectrum in the He I continuum (below 504 Å). Recent analysis (R. Gladstone et al. 2024) of the all-sky Ly α emission seen by the New Horizons spacecraft suggests that additional early B-type stars within the local hot bubble could contribute to the EUV radiation incident on the local clouds. Ionizing photons from these sources enter the local clouds from different directions, requiring 3D models of the radiative transfer and geometric structure of the local clouds².

Time-dependent effects. Most previous ionization models of the local ISM assumed equilibrium between photoionization and radiative recombination. However, over Myr timescales, these processes may not remain constant. Within the ensemble known as the CLIC or “complex of local interstellar clouds” (J. Slavin & P. Frisch 2002), the Sun’s motion of 25.7 km s^{−1} corresponds to 26.3 pc per Myr. Of the 15 clouds in the ISM within 15 pc (S. Redfield & J. Linsky 2008) two dominate the angular coverage on the sky: the local interstellar cloud (LIC) and the G cloud. The Blue cloud and Aql cloud are additional components of the local ISM (J. Linsky et al. 2019). P. Frisch (1994) suggested that the Sun entered the LIC within the last 10⁴ yr. Subsequent papers (J. Linsky et al. 2019; J. Linsky et al. 2022) argued that the Sun and its heliosphere may exit the LIC within the next 2000 yrs. P. Swaczyna et al. (2022) proposed that relative motions of LIC and G-cloud indicate a region of interaction.

Another characteristic dynamical time scale comes from the motion of ϵ CMa relative to the Sun.

$$t_{\text{star}} = d_*/V_* \approx (4.4 \text{ Myr}) \left(\frac{d_*}{124 \text{ pc}} \right) \left(\frac{V_*}{27.3 \text{ km s}^{-1}} \right)^{-1}.$$

From Hipparcos measurements (F. van Leeuwen 2007) its radial velocity is $V_* = 27.3 \pm 0.4 \text{ km s}^{-1}$ and its tangential velocity is $2.1 \pm 0.1 \text{ km s}^{-1}$. The latter velocity is based on its total proper motion $\mu_{\text{tot}} = 3.50 \pm 0.14 \text{ mas yr}^{-1}$ with components (in RA and Decl) of

²C. Gry & E. Jenkins (2014) suggested an alternative topology, in which the LIC and G-cloud are a single cloud, with internal velocity components arising from turbulence and a shock propagating through the cloud. S. Redfield & J. Linsky (2015) evaluated this alternative using additional sight lines and concluded that multiple clouds provide better kinematic agreement. J. Linsky & S. Redfield (2014) suggested cloud mixing along several sight lines along the axis between the LIC and G clouds. In our models, we treat absorption from the clouds as a single source of flux attenuation.

$\mu_\alpha \cos \delta = 3.24 \pm 0.11 \text{ mas yr}^{-1}$ and $\mu_\delta = 1.33 \pm 0.16 \text{ mas yr}^{-1}$. Approximately $4.4 \pm 0.1 \text{ Myr}$ ago, $\epsilon \text{ CMa}$ passed by the Sun at an offset distance of $9.3 \pm 0.5 \text{ pc}$, resulting in an ionizing radiation field 100–200 times higher than its current value. With the Sun’s current velocity setting it on a trajectory out of the local clouds, the location of $\epsilon \text{ CMa}$ relative to the local hydrogen gas remains uncertain. With a total mass of only 0.2–0.4 M_\odot , the local interstellar clouds within 3 pc are not self-gravitating and probably not gravitationally bound to the Sun. Thus, it is unclear whether they would be exposed to the same enhanced ionizing radiation. However, it is probable that $\epsilon \text{ CMa}$ produced considerable effects in its wake.

We now estimate the characteristic time scales for hydrogen photoionization and recombination, and for radiative cooling of gas at the cloud surface:

$$\begin{aligned} t_{\text{ph}} &= \Gamma_{\text{H}}^{-1} \approx (1.6 \text{ Myr}) \left(\frac{\Gamma_{\text{H}}}{2 \times 10^{-14} \text{ s}^{-1}} \right)^{-1} \\ t_{\text{rec}} &= (n_e \alpha_{\text{H}})^{-1} \approx (0.93 \text{ Myr}) \left(\frac{n_e}{0.1 \text{ cm}^{-3}} \right)^{-1} T_{7000}^{0.809} \\ t_{\text{cool}} &= \frac{3n_{\text{tot}}kT/2}{n_{\text{H}}^2 \Lambda(T)} \approx (11 \text{ Myr}) \left(\frac{n_{\text{H}}}{0.2 \text{ cm}^{-3}} \right)^{-1} T_{7000}. \end{aligned}$$

Here, we scaled Γ_{H} to the estimated EUV continuum outside the LIC and adopted a case-B radiative recombination rate coefficient $\alpha_{\text{H}} = (3.39 \times 10^{-13} \text{ cm}^3 \text{ s}^{-1}) T_{7000}^{-0.809}$ (B. Draine 2011), appropriate for $T = (7000 \text{ K}) T_{7000}$. We adopted total hydrogen density $n_{\text{H}} \approx 0.2 \text{ cm}^{-3}$, electron density $n_e \approx 0.1 \text{ cm}^{-3}$, and a radiative cooling rate $n_{\text{H}}^2 \Lambda(T)$ with coefficient $\Lambda(T) \approx 3 \times 10^{-26} \text{ erg cm}^3 \text{ s}^{-1}$ at 7000 K. The radiative cooling time and stellar crossing time are both longer than the time needed to establish photoionization equilibrium.

Approximately 4.4 Myr ago, $\epsilon \text{ CMa}$ passed within 9–10 pc of the Sun, with a photoionization rate 180 times higher than at present. Any gas clouds in the Sun’s vicinity at that time would have been highly ionized. In fact, $\epsilon \text{ CMa}$ may have left a wake of ionized and photoelectrically heated gas, which could explain the tunnel of low N_{HI} in this direction. Because $t_{\text{ph}} \approx t_{\text{rec}}$, an equilibrium level of ionization was established, evolving on Myr timescales tracking the B-star’s motion. In the future, the Sun will exit the local cloud and once again be exposed to a much higher ionizing radiation field unshielded by the local cloud.

We thank the referee for comments on the spectral classification and suggestions on information displayed in figures. We also thank Edward Jenkins for a thorough discussion of HST absorption-line studies of the sight line to $\epsilon \text{ CMa}$, including conversations at the Berkeley conference just two months before his decease. His wisdom and contributions to studies of interstellar matter will be greatly missed. We also thank James Green and Nick Erickson for access to their flux-calibrated EUV and FUV spectra of $\epsilon \text{ CMa}$, and Cecile Gry,

Jeffrey Linsky, Seth Redfield, and Jon Slavin for scientific discussions about the local ISM. John Hillier, Ivan Hubeny, and Tadziu Hoffmann kindly provided useful information about their model atmosphere codes. A portion of this study was supported by the New Horizons Mission calibration observations of ϵ CMa and studies of cosmic UV and Ly α backgrounds.

REFERENCES

- Bethe, H. A., & Salpeter, E. E. 1957, *Quantum Mechanics of One- and Two-Electron Atoms* (Berlin: Springer)
- Bohlin, R. C. 1975, *ApJ*, 200, 402
- Bohlin, R. C., Savage, B. D., & Drake, J. F. 1978, *ApJ*, 224, 132
- Bowen, D. V., Jenkins, E. B., Tripp, T. M., et al. 2008, *ApJS*, 176, 59
- Brott, L., de Mink, S. E., Cantiello, M., et al. 2011, *A&A*, 530, A115
- Cassinelli, J. P., Cohen, D. H., MacFarlane, J. J., et al. 1995, *ApJ*, 438, 932
- Code, A. D., Davis, J., Bless, R. C., & Hanbury Brown, R. 1976, *ApJ*, 203, 417
- Deng, L., & Xiong, D. R. 2001, *MNRAS*, 327, 881
- Draine, B. T. 2011, *Physical Processes in the Interstellar and Intergalactic Medium* (Princeton: Princeton Univ. Press)
- Dupuis, J., Vennes, S., Bowyer, S., Pradhan, A. K., & Thejll, P. 1995, *ApJ*, 455, 574
- Erickson, N., Green, J., Nell, N., et al. 2021, *J. Astron. Telesc. Instrum. Syst.*, 7.1.015002
- Ferlet, R. 1981, *A&A*, 98, L1
- Fossati, L., Castro, N., Morel, T., et al. 2015, *A&A*, 574, A20
- Frisch, P. C. 1994, *Science*, 265, 1423
- Georgy, C., Ekström, S., Granada, A., et al. 2013, *A&A*, 553, A24
- Gladstone, G. R., Shull, J. M., Pryor, W. R., et al. 2024, *ApJ*, submitted
- Gry, C., & Jenkins, E. B. 2001, *A&A*, 367, 617
- Gry, C., & Jenkins, E. B. 2014, *A&A*, 507, A58
- Gry, C., Lemonon, L., Vidal-Madjar, A., Lemoine, M., & Ferlet, R. 1995, *A&A*, 302, 497
- Hanbury Brown, R., Davis, J., & Allen, L. R. 1974, *MNRAS*, 167, 121
- Hillier, D. J., & Miller, D. L. 1998, *ApJ*, 496, 407
- Hubeny, I., Hummer, D. G., & Lanz, T. 1994, *A&A*, 282, 15

- Jenkins, E. B., Oegerle, W. R., Gry, C., et al. 2000, *ApJ*, 538, L81
- Kurucz, R. L. 1979, *ApJS*, 40, 1
- Leitherer, C., Schaerer, D., Goldader, J. D., et al. 1999, *ApJS*, 123, 3
- Leitherer, C., Ekström, S., Meynet, G., et al. 2014, *ApJS*, 212, 14
- Lesh, J. R. 1968, *ApJS*, 17, 371
- Lesh, J. R. 1972, *A&AS*, 5, 129
- Linsky, J. L., Redfield, S., & Tilipman, D. 2019, *ApJ*, 886, 41
- Linsky, J. L., Redfield, S., Ryder, D., & Möbius, E. 2022, *Space Science Reviews*, 218, 16
- Linsky, J. L., & Redfield, S. 2024, preprint
- Martins, F., Schaerer, D., & Hillier, D. J. 2005, *A&A*, 436, 1049
- Najarro, F., Kudritzki, R. P., Cassinelli, J. P. et al. 1996, *A&A*, 306, 892
- Negueruela, I., Simón, S., de Burgos, A., Casasbuenas, A., & Beck, P. G. 2024, *A&A*, 690, A176
- Nieva, M.-F., & Przybilla, N. 2012, *A&A*, 539, A143
- Osterbrock, D. E., & Ferland, G. 2006, *Astrophysics of Gaseous Nebulae and Active Galactic Nuclei* (Sausalito: University Science Books)
- Pauldrach, A. W. A., Hoffmann, T. L., & Lennon, M. 2001, *A&A*, 275, 161
- Pederson, M. G., Escorza, A., Pápics, P., & Aerts, C. 2020, *MNRAS*, 495, 2738
- Redfield, S., & Linsky, J. L. 2008, *ApJ*, 673, 283
- Redfield, S., & Linsky, J. L. 2015, *ApJ*, 818, 125
- Samson, J. A. R., He, Z. H., Yin, L., & Haddad, G. N. 1994, *J Phys B*, 27, 887
- Savage, B. D., Bohlin, R. C., Drake, J. F., & Budich, W. 1977, *ApJ*, 216, 291
- Slavin, J. D., & Frisch, P. C. 2002, *ApJ*, 565, 364
- Snow, T. P., & Morton, D. C. 1976, *ApJS*, 32, 429
- Swaczyna, P., Schwadron, N. A., Möbius, E., et al. 2022, *ApJ*, 937, L32
- Topping, M. W., & Shull, J. M. 2015, *ApJ*, 800, 97
- Vallerga, J. V. 1998, *ApJ*, 497, 921
- Vallerga, J. V., & Welsh, B. Y. 1995, *ApJ*, 444, 702
- van Leeuwen, F. 2007, *A&A*, 474, 653

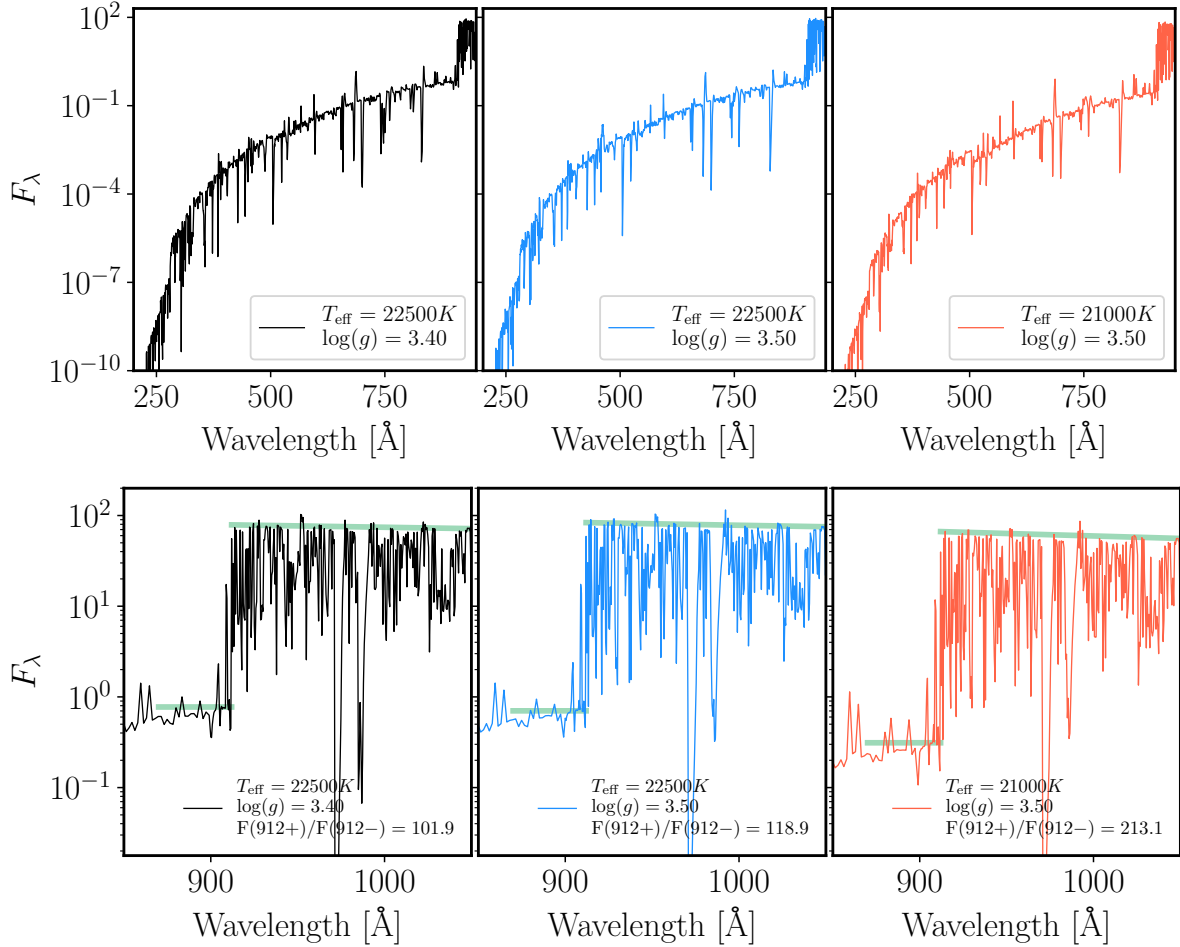


Fig. 3.— (Top panels). Far-UV and EUV spectra from three model atmospheres for ϵ CMa, computed with the non-LTE line-blanketed code **WM-basic** and plotting the flux distribution $\log F_\lambda$. Two models use the elevated effective temperature $T_{\text{eff}} = 22,500$ K and surface gravities $\log g = 3.40$ and 3.50 . A third model uses $T_{\text{eff}} = 21,000$ K based on integrated-flux bolometry (A. Code et al. 1976). The absence of a He I edge (504 \AA) may result from back-warming of the upper atmosphere by a line-blanketed stellar wind. (Bottom panels.) Zoom-in plots of flux decrements $F(912^+)/F(912^-)$ at the Lyman edge. These factors are $\Delta_{\text{LL}} = 102$ and 119 for the two $22,500$ K models and $\Delta_{\text{LL}} = 213$ for the $21,000$ K model.

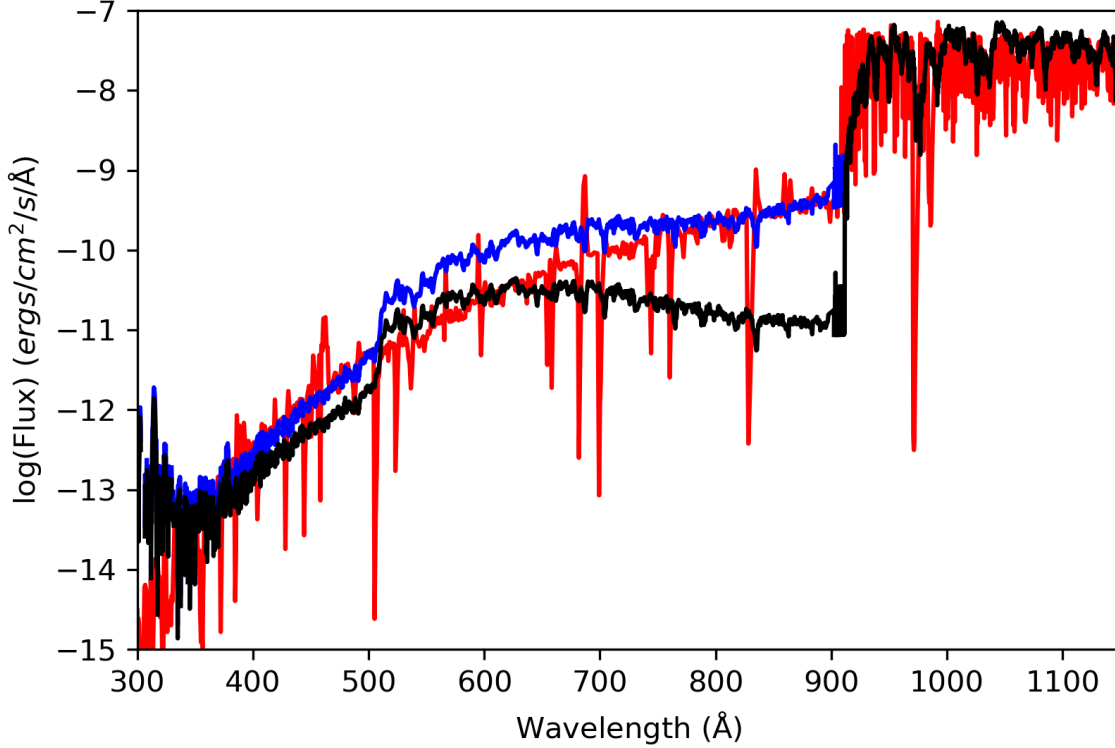


Fig. 4.— We illustrate the combined attenuation of the EUV continuum of ϵ CMa by both the stellar atmosphere and ISM. The red curve shows the `WM-basic` model atmosphere spectrum ($T_{\text{eff}} = 22,500$ K and $\log g = 3.50$) overlaid on the observed EUV/FUV spectrum (black curve). The flux-restored spectrum (blue) assumes an intervening H I column density $N_{\text{HI}} = 6 \times 10^{17} \text{ cm}^{-2}$, with optical depth $\tau_{\text{LL}} = 3.8 \pm 0.1$ at the Lyman edge. The observed spectrum has a total LL flux decrement $\Delta_{\text{LL}} = F(912^+)/F(912^-) = 5000 \pm 500$. Our model has a stellar decrement $\Delta_{\text{star}} = 110 \pm 10$ and an ISM decrement $\Delta_{\text{ISM}} = 45 \pm 5$.

Table 1. Various Stellar Parameters^a

Reference Paper	d (pc)	T_{eff} (K)	$\log g$ (cgs)	R/R_{\odot}	M/M_{\odot}	L/L_{\odot}	M_{bol} (mag)
Snow & Morton (1976)	...	20,990	3.20	16.6	16	47,400	−6.95
Cassinelli et al. (1995)	188	$20,990 \pm 760$	3.20 ± 0.15	$16.2^{+1.2}_{-1.2}$	$15.2^{+6.4}_{-4.4}$	$45,900 \pm 9500$	−6.91
Fossati et al. (2015) ^b	124 ± 2	$22,500 \pm 300$	3.40 ± 0.08	$12.0^{+1.7}_{-1.5}$	$13.1^{+1.0}_{-0.9}$	$33,250^{+9600}_{-8500}$	−6.56
Fossati et al. (2015) ^c	124 ± 2	$22,500 \pm 300$	3.40 ± 0.08	$10.1^{+0.7}_{-0.5}$	$12.0^{+0.4}_{-0.4}$	$23,550^{+3500}_{-2650}$	−6.19
Erickson et al. (2021)	124 ± 2	$22,500 \pm 300$	3.40 ± 0.08	$12.0^{+1.7}_{-1.5}$	$13.1^{+1.0}_{-0.9}$	$33,250^{+9600}_{-8500}$	−6.56
Current Study (2024)	124 ± 2	$21,000 \pm 780$	3.50 ± 0.05	10.7 ± 0.7	13.1 ± 2.4	$19,900 \pm 1600$	−5.97

^aValues of effective temperature, surface gravity, radius, mass, luminosity, and bolometric absolute magnitude given in various papers. L. Fossati et al. (2015) derived R and M from two sets of evolutionary tracks (see footnote b).

^bStellar mass and radius inferred from evolutionary tracks of C. Georgy et al. (2013).

^cStellar mass and radius inferred from evolutionary tracks of L. Brott et al. (2011).

Table 2. Estimated H I Column Densities^a

Reference Paper	N_{HI} (cm^{-2})	Method
J, Cassinelli et al. (1995)	$(7\text{--}12) \times 10^{17}$	LyC (EUV-flux) modeling
C. Gry et al. (1995)	$< 5 \times 10^{17}$	N I absorption ($\text{N}/\text{H} = 6.76 \times 10^{-5}$)
C. Gry & E. Jenkins (2001)	$(3.1\text{--}3.7) \times 10^{17}$	N I absorption ($\text{N}/\text{H} = 7.5 \times 10^{-5}$)
C. Gry & E. Jenkins (2001)	$(7\text{--}11) \times 10^{17}$	O I absorption ($\text{O}/\text{H} = 3.16 \times 10^{-4}$)
C. Gry & E. Jenkins (2001)	$(4.8\text{--}7.2) \times 10^{17}$	O I absorption ($\text{O}/\text{H} = 4.68 \times 10^{-4}$)
Current Study	$(6 \pm 1) \times 10^{17}$	LyC restoration + Model Atmospheres

^aPrevious estimates of intervening column density of H I. Methods include modeling the attenuation of stellar EUV fluxes and scaling N_{HI} from column densities of N I or O I, with assumptions about their interstellar abundances and depletion factors. The two values reported by C. Gry & E. Jenkins (2001) from O I are based on different assumed (O/H) abundances in the ISM (3.16×10^{-4}) and in local B-stars (4.68×10^{-4}). C. Gry & E. Jenkins (2001) suggested that nitrogen may be underabundant relative to solar values. There could also be variations in the ionization fractions of N, O, H, and He, owing to photoionization cross sections and charge exchange rates (O I and N I).

Table 3. Lyman Decrements and Photoionization Rates^a

N_{HI} (cm^{-2})	Δ_{LL} (ISM)	Φ_{LyC} ($\text{cm}^{-2} \text{ s}^{-1}$)	Γ_{H} (s^{-1})	x_{s} (0.2 cm^{-3})	x_{s} (0.1 cm^{-3})
0 (no abs)	1.00	300	9.85×10^{-16}	0.108	0.150
3.0×10^{17}	6.62	883	3.35×10^{-15}	0.191	0.258
5.0×10^{17}	23.3	2000	8.25×10^{-15}	0.282	0.373
6.0×10^{17}	43.8	3090	1.33×10^{-14}	0.342	0.445
6.5×10^{17}	60.0	3870	1.69×10^{-14}	0.376	0.484
7.0×10^{17}	82.3	4870	2.17×10^{-14}	0.413	0.525
8.0×10^{17}	154	7810	3.58×10^{-14}	0.493	0.611
9.0×10^{17}	290	12,700	6.00×10^{-14}	0.581	0.698

^aFor the published range of interstellar column densities N_{HI} , we present our modeled interstellar flux decrement $\Delta_{\text{LL}} = \exp(-\tau_{\text{LL}})$ for optical depth τ_{LL} , integrated photon flux Φ_{LyC} in the Lyman continuum, and photoionization rate Γ_{H} . The last columns show the hydrogen ionization fraction, x_{s} , at the cloud surface for two values, 0.2 cm^{-3} and 0.1 cm^{-3} , of total hydrogen density, $n_{\text{H}} = n_{\text{HI}} + n_{\text{HII}}$. We assume equilibrium $x^2/(1-x) = (\Gamma_{\text{H}}/1.1n_{\text{H}}\alpha_{\text{H}})$ with recombination rate coefficient $\alpha_{\text{H}} = 3.39 \times 10^{-13} \text{ cm}^3 \text{ s}^{-1}$ at $T = 7000 \text{ K}$.